

# A low-cost ice melt monitoring system using wind-induced motion of mass-balance stakes

Felix St-Amour<sup>1</sup>, H. Cynthia Chiang<sup>1,2</sup>, Jamie Cox<sup>1</sup>, Eamon Egan<sup>1</sup>, Ian Hendrickson<sup>1,2</sup>, Jonathan Sievers<sup>1,2</sup>, and Laura Thomson<sup>3</sup>

<sup>1</sup>Department of Physics, McGill University, Montreal, Canada

<sup>2</sup>Trottier Space Institute, McGill University, Montreal, Canada

<sup>3</sup>Department of Geography and Planning, Queen's University, Kingston, Canada

**Correspondence:** Felix St-Amour (felix.st-amour@mail.mcgill.ca)

## Abstract.

Surface ablation measurements of glaciers are critical for understanding mass change over time. Mass-balance stakes are commonly used for localized measurements, with the exposed length typically measured manually at infrequent intervals. This paper presents the design and validation of new instrumentation that automates mass-balance stake readings, thus enabling continuous measurements with high temporal resolution. The instrumentation comprises readout electronics that are mounted on mass-balance stakes to measure wind-induced vibrations. The stake vibrational frequency depends sensitively on the exposed length, and changes in the measured frequency therefore are indicative of glacier surface melt and accumulation. Initial instrumentation field tests conducted at Color Lake on Umingmat Nunaat (Axel Heiberg Island), Nunavut, demonstrate centimeter-level precision on length measurements. The instrumentation can be attached to existing mass-balance stakes and is low-cost ( $\sim \$50$  USD) in comparison to many other systems that perform automated surface ablation measurements. The accessibility of this instrumentation opens new possibilities for localized, high temporal resolution measurements of glacier surface activity at any locations where mass balance stakes are deployed.

## 1 Introduction

Glaciers and ice caps, recognized indicators of a changing climate, have exhibited continued and often accelerated mass loss through the early 21st century (e.g., Hugonnet et al. (2021)). These changes have strong implications for sea level rise, and for communities and ecosystems impacted by runoff (Immerzeel et al., 2020). The glaciological mass balance method (e.g., Østrem and Stanley (1966)) is one approach used to quantify annual changes within a glacier system, using an input-output approach that interpolates and extrapolates measurements of mass gain (primarily snow accumulation) and mass loss (primarily ice melt and iceberg calving) across the glacier to gain a glacier-wide mass change commonly reported in meters of water equivalent (Cogley et al., 2010). Point measurements of accumulation are made from measurements of snow thickness and density in snow pits, while ice melt is most commonly determined from measuring the exposure of mass-balance stakes drilled into the ice. Measurements for mass balance are most generally made only once or twice per year, representing annual or seasonal summer and winter balances, respectively (Cogley et al., 2010). While this observation frequency is sufficient for standardized

mass balance reporting, there is an increasing demand for data with higher temporal resolution to support and improve mass balance projections and runoff models. For most glacierized regions in the world, including the Canadian Arctic, ice melt is the dominant control on annual mass balance (Sharp et al., 2011). Therefore, continuous melt monitoring can serve as a valuable, real-time, indicator of mass balance conditions and can support timely runoff projections for downstream environments and communities.

Continuous ice melt monitoring has previously been demonstrated by several systems employing a wide range of technologies. Wickert et al. (2023) developed an ablation stake system with a downward-looking ultrasonic rangefinder to measure the distance to the glacier surface, with an estimated cost of \$700 USD per instrument. Landmann et al. (2020) present a camera-based pole monitoring system, which was later upgraded to use computer vision to automate melt measurements (Cremona et al., 2023). While the camera system is able to determine surface height changes with millimeter-level precision, high ablation rates can cause misreadings. Carturan et al. (2019) used a string of thermistors to directly measure melt activity, with linear resolution ( $\pm 3$  cm) determined by the spacing between thermistors. Hulth (2010) presents a draw-wire method, although the measurement is sensitive to only surface lowering and not accumulation. Bøggild et al. (2004) created a pressure transducer ice melt monitoring system that is well suited for high ablation regions, although snow accumulation complicates the measurements.

This study, inspired by the resonating rainfall and evaporation recorder developed by Stewart et al. (2012), presents the development of new instrumentation that continuously monitors mass-balance stake exposure by recording wind-induced vibrational frequency. The frequency depends sensitively on the exposed length, allowing centimeter-level measurement precision (and sometimes better, depending on operating conditions). The instrumentation is designed to run autonomously in Arctic environmental conditions for up to several years while taking hourly measurements. In comparison to other existing technologies for automated measurements, the system presented here is low-cost and can be attached to mass-balance stakes that are already installed in the field. This paper describes the instrument design, the derivation of exposed stake length from vibrational frequency, data analysis methods, lab tests, and initial Arctic field tests.

## 2 BRACHIOSAURUS design

The Boxed Recorder Analyzing the Change in Height of Ice with On-Site Accelerometer and Ultrasonic Readers Utilizing Support (BRACHIOSAURUS, or BRACHI for short) consists of an electronics box that is attached to the top of a mass-balance stake, as shown in Figure 1 (a). A microcontroller receives the data from an accelerometer, a temperature sensor, and a depth sensor (Figure 1 (b)). The hardware design files, control code, and analysis software are all open source and available online. Each of the BRACHI components are described in detail below.

### 2.1 Accelerometer and temperature sensor

The vibrations of the mass-balance stake are measured by an LSM6DSOX inertial measurement unit that has a three-axis accelerometer and a temperature sensor. The unit's accelerometer has a full-scale range of  $\pm 16$  g and a specified operating

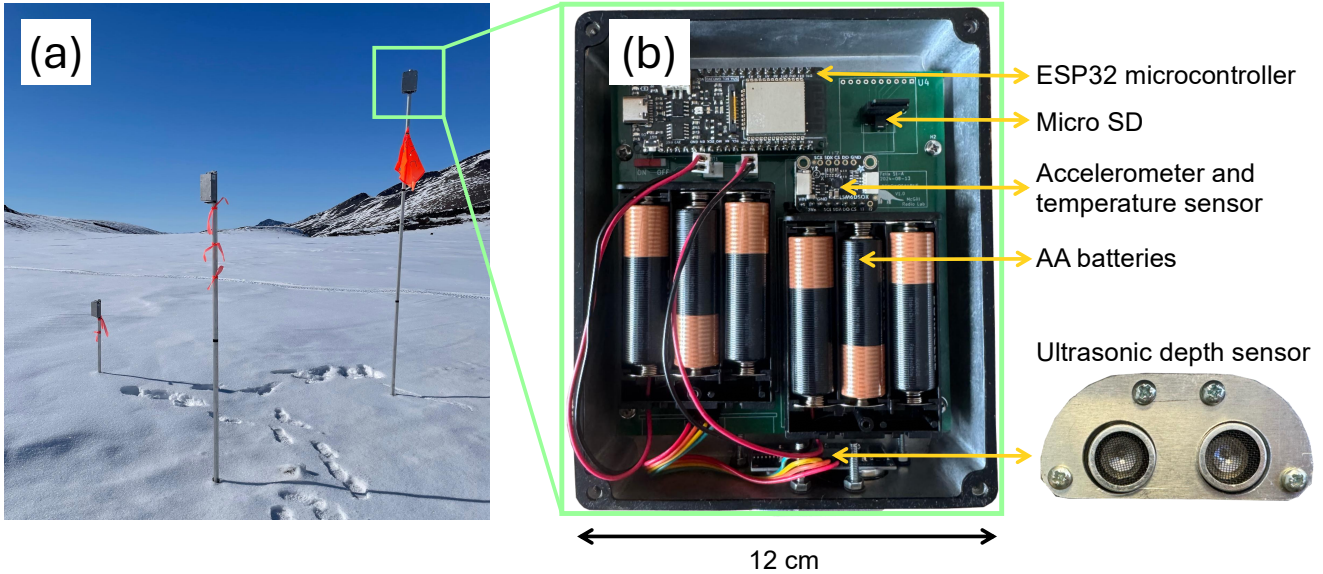


**Figure 1.** (a) The BRACHI electronics box attaches to the top of a mass-balance stake. The three units in this photo were tested at Color Lake on Axel Heiberg Island in May 2025, using stakes frozen into the lake surface at varying exposed lengths (1, 2, and 3 meters). (b) The BRACHI electronics include an accelerometer with an integrated temperature sensor, downward-facing depth sensor, microcontroller, micro-SD card, and AA batteries. The components are mounted on a custom circuit board and housed inside a weatherproof enclosure.

temperature range of  $-40^{\circ}\text{C}$  to  $85^{\circ}\text{C}$ . The temperature sensor data are saved by BRACHI, and the readings are also used internally by the LSM6DSOX to correct for accelerometer drift. The temperature readings are typically  $0^{\circ}\text{C}$  to  $5^{\circ}\text{C}$  higher than ambient since the sensor is sheltered inside the enclosure with powered electronics. Temperature readings can also be used to correct changes in the stiffness of the metal stake; however, these corrections are negligible for typical operating conditions (for aluminum, the stiffness varies by 3% between  $-40^{\circ}\text{C}$  and  $20^{\circ}\text{C}$ , which corresponds to a difference of 1% on derived stake length).

## 2.2 Depth sensor

An HC-SR04 ultrasonic sensor is affixed to a custom metal cutout and mounted at the bottom of the enclosure, facing downward to measure the distance to the top surface of the glacier. Although the HC-SR04 is rated to only  $-20^{\circ}\text{C}$  and has a limited range of 4 m, it costs only  $\sim \$3$  USD. Other ultrasonic sensors with wider temperature ratings and longer distance sensing are typically at least  $\sim 10$  times more expensive and would nearly double the total BRACHI cost. The HC-SR04 is therefore used intentionally in an opportunistic manner, rather than providing a primary source of data. When operating conditions permit, the ultrasonic sensor provides an affordable and valuable cross-check against stake lengths derived from the accelerometer data.

## 2.3 Microcontroller and data storage

BRACHI employs an ESP32 microcontroller module, model DFR0654, to read and process sensor data. The raw data are saved to a micro SD card. The ESP32 was chosen for its  $-40^{\circ}\text{C}$  rating, computational power for the required onboard data processing, ability to enter a low power state while drawing only tens of  $\mu\text{A}$ , and embedded wireless capability. The wireless access point enables users to remotely download data, rather than directly accessing the micro SD. The micro SD is a 4-GB Delkin Devices Utility+ (S304GSEMC-U3000-3) and is rated to  $-40^{\circ}\text{C}$ . The BRACHI control code is written in the Arduino programming language.

## 2.4 Batteries

BRACHI is powered by six AA batteries connected in two parallel strings of three cells each. With the estimated power draw of the readout electronics under normal operations, a set of six 3000-mAh lithium batteries is expected to last for a minimum of three years. Lithium batteries are used for their survivability at subzero temperatures.

## 2.5 Circuit board and enclosure

The BRACHI electronics are mounted on a custom printed circuit board, which is rigidly attached to the surrounding enclosure. The enclosure is an aluminum box that is made waterproof with a rubber gasket under the lid, o-rings beneath each screw, and additional o-rings surrounding the depth sensor “eyes.” The enclosure is attached to the stake with U-bolts. The total weight of the BRACHI system (including U-bolts and batteries) is approximately 0.68 kg.

## 3 Vibrational frequency and exposed stake length

The relationship between vibrational frequency and length is obtained by modeling a BRACHI-equipped stake as a cylindrical Euler–Bernoulli beam with a point mass at its free end, as illustrated in Figure 2. The basic equations that govern this system are available in engineering textbooks, e.g., Blevins (1979, ch. 8) and Stokey (2002, ch. 7). The first, or fundamental, vibrational mode of the stake corresponds to back-and-forth swaying motion along the entire length. A simplified expression for the associated vibrational frequency, assuming a point mass at the end of the stake, is given by

$$F_1(L) = \frac{1}{2\pi} \sqrt{\frac{3E\frac{\pi}{4}(R^4 - r^4)}{L^3[m + 0.24\pi L\rho(R^2 - r^2)]}}. \quad (1)$$

Here  $L$  is the exposed stake length,  $E$  is the Young’s modulus of the stake material,  $R$  and  $r$  are the respective outer and inner stake radii,  $m$  is the mass of BRACHI, and  $\rho$  is the density of the stake material. The treatment of  $m$  as an extended mass is discussed in Appendix A, and the solution for  $F_1$  must be obtained numerically.

In principle, the stake can also support higher-order vibrational modes. We have found that the second mode is often excited in our particular setups; this motion corresponds to bending of the stake with one stationary node near the top. The frequencies

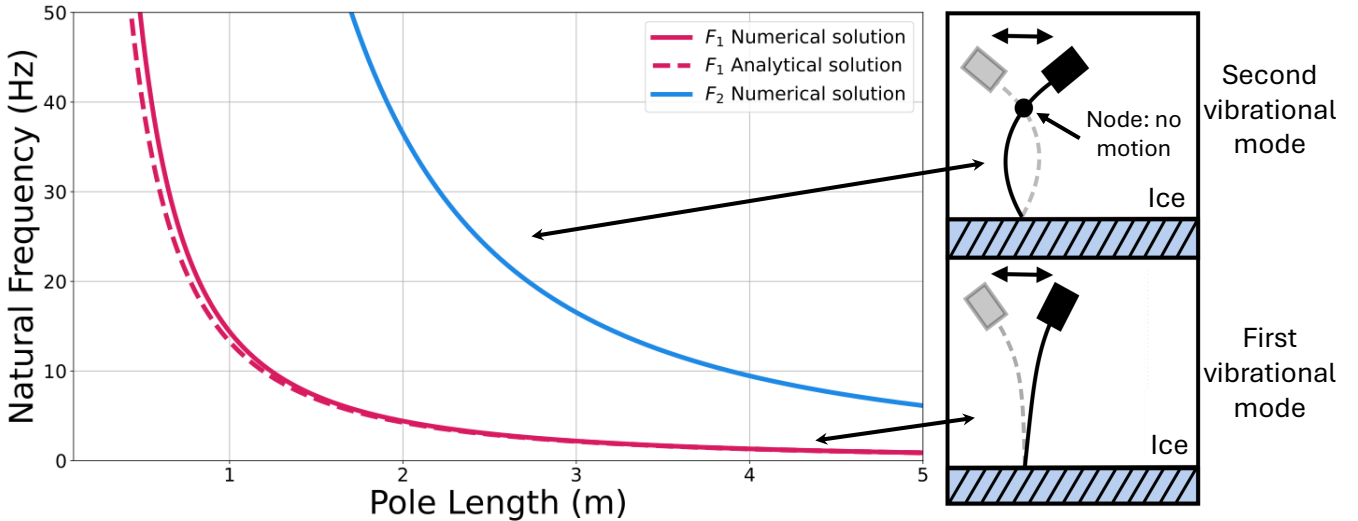


**Figure 2.** A BRACHI-equipped stake is modeled as a vertical beam with a mass on the top end. Vibrational frequency as a function of exposed stake length is plotted for the first and second vibrational modes, and the corresponding stake motions are illustrated in the insets. The slight difference between the numerical and analytic solutions for  $F_1$  arises from treating BRACHI as an extended or point mass, respectively.

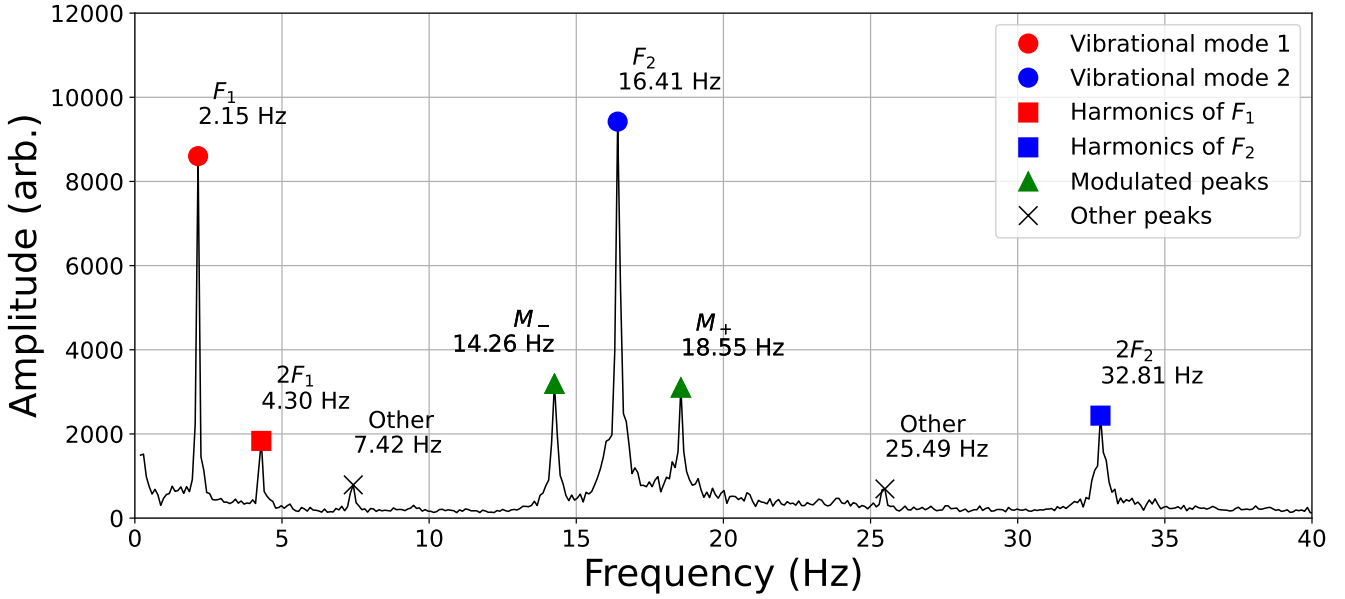
of the second and higher-order modes do not have analytic expressions but can be obtained numerically (Erturk and Inman, 2011), with details given in Appendix A.

Figure 2 shows the numerically computed frequency–length relationship for the first two vibrational modes of an example BRACHI-equipped stake, along with the analytic prediction from Eq. (1). (The detailed stake parameters are given in §6.) A small discrepancy between the analytic and numerical solutions for  $F_1$  is visible at  $\lesssim 1$  m and arises from the differences in assuming an extended (numerical solution) or point mass (analytical solution) for BRACHI. In the remainder of this work, numerical solutions including an extended mass will be used for computing lengths from vibrational frequency measurements.

#### 4 Data acquisition and analysis methods

The BRACHI firmware is configurable to allow user-defined data collection schedules. For the tests presented in this paper, data are recorded for 120 seconds every hour. The three-axis accelerometer is sampled at 200 Hz, and to reduce data volume, the acceleration is squared and summed across all three axes before being saved to the micro SD card. The acceleration data are processed offline to determine the stake length as a function of time. Processing of each 120-second timestream begins with dividing the data into 10 equal-length chunks. Analyzing these chunks enables identification of low-amplitude vibrational modes that may fluctuate above and below the noise floor. Each chunk is Fourier transformed and squared to obtain a power spectrum, where the vibrational frequencies of the stake appear as narrow peaks.

Figure 3 shows all of the frequency peaks that are typically present, although for some measurements under different conditions, only a subset of these frequencies may be excited at detectable levels. The peaks in the power spectrum include the



**Figure 3.** An example power spectrum of accelerometer data from a BRACHI unit on a 3-m stake installed on a frozen lake. The first and second vibrational modes appear as the largest peaks in the spectrum at  $F_1$  and  $F_2$ . Additional spectral lines are visible at  $2F_1$ ,  $2F_2$ , and  $F_2 \pm F_1$ . Other peaks without a harmonic relationship to  $F_1$  and  $F_2$  are considered spurious and are excluded from analysis.

first and second vibrational modes ( $F_1$  and  $F_2$ ) and other spectral lines at  $2F_1$ ,  $2F_2$ , and  $F_2 \pm F_1$ . The peaks at  $2F_1$ ,  $2F_2$ , and  $F_2 \pm F_1$  arise from Fourier transforming the squared magnitude of the acceleration. Future measurements will save and process the motion of all axes separately without squaring.

In a single power spectrum measurement, peaks are located by searching for local maxima that lie above the noise floor. Identification of these peaks begins with finding a candidate  $F_1$ , determined by the peak location with the highest amplitude within a frequency range of 0 to  $2F_1$ . Then,  $F_2$  is identified by searching for a set of three peaks located at  $F_2 - F_1$ ,  $F_2$ , and  $F_2 + F_1$ . Candidate  $F_1$  and  $F_2$  frequencies are computed for all chunks, and the values that are most consistent across the chunks are averaged together for the data recording period. The error on each averaged frequency measurement is taken to be the larger of the computed error on the mean, or the frequency resolution of the spectrum. The averaged  $F_1$  and  $F_2$  values are each used to compute  $L$ , and a weighted average of those  $L$  values yields the final length measurement of the stake. The error on  $L$  is obtained by numerically propagating the errors from  $F_1$  and  $F_2$ .

## 5 Laboratory measurements

BRACHI was initially tested by clamping a mass-balance stake at various points along its length against a table and manually inducing vibration. Length measurements were calculated from accelerometer data using the methods described in §4. The stake used for initial testing was a hollow tube made of aluminum T6061 with assumed values of  $E = 69$  GPa and  $\rho = 2.7$  g/cm

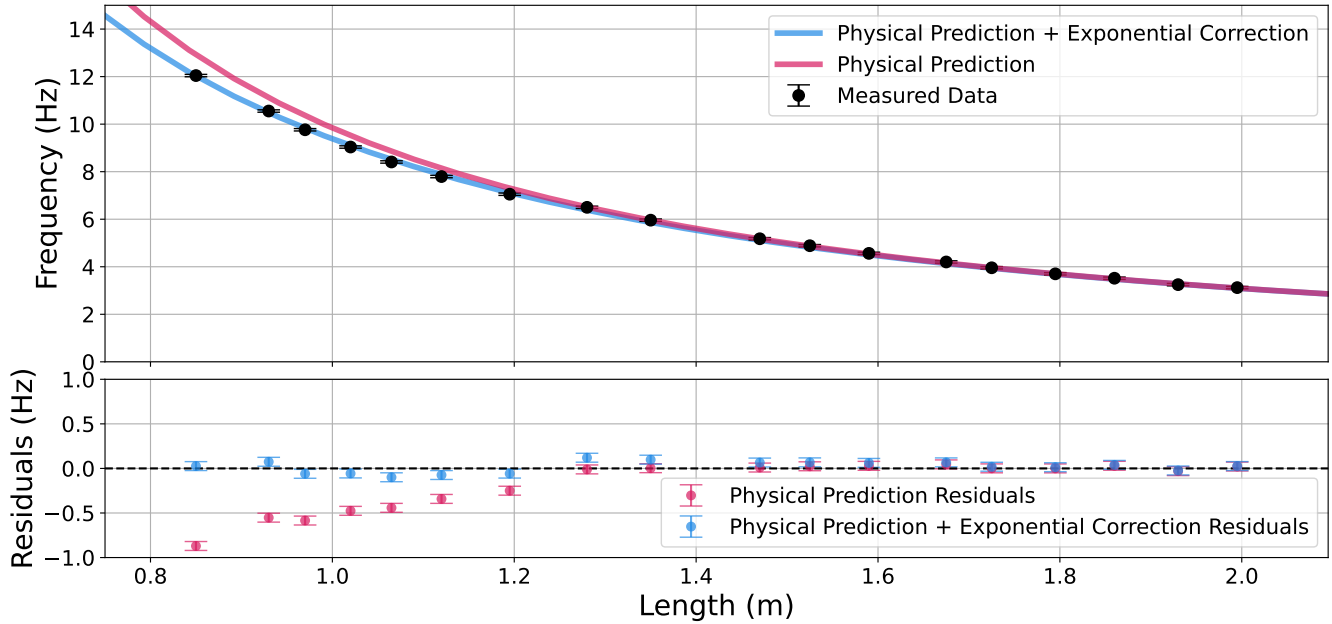


**Figure 4.** Frequency versus length for the first vibrational mode of a BRACHI-equipped mass-balance stake that was tested in the lab. The stake was clamped at varying points to change the effective length, and vibrations were induced manually. Lengths derived from BRACHI accelerometer data agree well with the physical prediction at  $\gtrsim 1.2$  m. At shorter lengths, an exponential correction can be applied to improve the fit and quantify systematic errors.

(Summers et al., 2015). The outer and inner radii were respectively measured as  $1.28 \pm 0.02$  cm and  $1.02 \pm 0.02$  cm with calipers. The BRACHI mass was measured as  $677 \pm 1$  g with a scale.

Figure 4 shows the measured frequencies of the first vibrational mode against the derived lengths, compared with the physical prediction. The measured and predicted frequencies agree within  $\sim 0.1$  Hz for lengths above 1.2 m, but the differences increase at shorter lengths. This discrepancy may arise from limitations of the lab setup such as non-rigidity in the clamping point, which effectively increases the stake length and lowers the vibrational frequency. The Euler–Bernoulli model may also lose accuracy at short lengths, and alternate models such as Timoshenko (1922) may provide better results for shorter stakes.

The difference between the data and prediction can be characterized using an additive exponential correction of the form  $Ae^{BL}$ , where  $A$  and  $B$  are nuisance parameters. Including this correction improves the agreement at shorter stake lengths, and the fitted exponential can be used to quantify systematic errors. Although we demonstrate the improved fit with lab data, we find that the correction is unnecessary for our field data (§6) because the stake is seated more rigidly when embedded in ice, and most of the measurements use stakes with an exposed length of  $> 1$  m.

Figure 5 shows the difference between BRACHI-derived lengths and direct length measurements obtained with a tape measure. The length measurements agree well above  $\sim 1.2$  m, with no systematic offset, a mean absolute error of 0.5 cm, and root mean square error of 0.7 cm. Including the exponential correction term yields similar accuracy below 1.2 m. As the

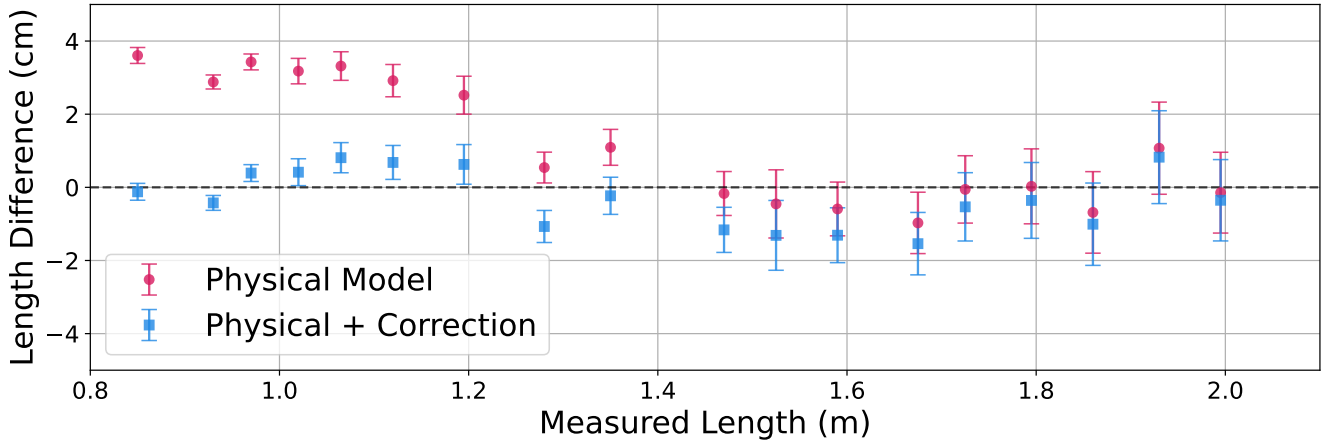


**Figure 5.** Differences between lengths derived from accelerometer data and lengths obtained directly with a tape measure for a BRACHI-equipped mass-balance stake in the lab. The length measurements agree with a maximum absolute error of 0.5 cm at  $\gtrsim 1.2$  m, and including an exponential correction yields similar errors at shorter lengths.

stake length increases, the error bars widen because the frequency–length relation for the first vibrational mode flattens, making the derived length more sensitive to small deviations in the estimated frequency. Analysis of higher-order modes, if present in the data, may help improve the errors because of the steeper frequency–length relation. Overall, the lab measurements demonstrate that BRACHI data constrain stake length with sub-centimeter accuracy and centimeter-level precision. These estimates are slightly conservative because they include the error of the tape measure (estimated precision of 0.25 cm).

Although the depth sensor was tested qualitatively in the lab, the detailed accuracy and precision were not measured because the stake was not attached to a flat horizontal surface. The depth sensor datasheet reports an accuracy of 3 mm, and the vertical position of the sensor within the BRACHI enclosure was measured with a precision of 2 mm. These estimates are included in the depth sensor errors from field data.

## 6 Arctic field tests

In May 2025, the BRACHI system was tested on three mass-balance stakes that were frozen into the ice of Color Lake at the McGill Arctic Research Station (Pollard et al., 2009) on Umingmat Nunaat (Axel Heiberg Island), Nunavut. The purpose of this test was to validate BRACHI performance in Arctic field conditions, using a controlled ice surface that would stay at a nearly constant level over a week-long observation period. The stakes were embedded in the ice with nominal exposed lengths of 1, 2, and 3 m.

**Table 1.** Comparison of stake lengths obtained with a measuring tape, accelerometer data (with the first and second vibrational modes analyzed separately), and depth sensor data. Measurements are presented for three different stakes over a two-hour test window.

Measuring tape [cm]	Accelerometer $F_1$ [cm]	Accelerometer $F_2$ [cm]	Depth sensor [cm]
99	$102.4 \pm 0.1$	–	$99.4 \pm 0.5$
200	$199.2 \pm 0.2$	$199.0 \pm 0.1$	–
300	$303.6 \pm 0.4$	$302.1 \pm 0.1$	–

## 6.1 BRACHI comparison against direct length measurements

To assess the accuracy of BRACHI, lengths derived from accelerometer data and the depth sensor were compared against lengths obtained directly with a tape measure. This test was conducted over a two-hour period when the ambient temperature was below freezing and at a local minimum. The short period of data collection ensures a stable operating environment while probing instrument accuracy, and the low temperature ensures that the ice surrounding the stake is solid. For this test, BRACHI was configured to record 120 seconds of data every 15 minutes, rather than every hour. Table 1 presents the comparison of measured lengths. The first and second vibrational modes of the accelerometer data are analyzed separately to assess consistency in derived lengths. During this short test, not all BRACHI length measurements were successfully recorded. The wind at the time did not excite the second vibrational mode in the 1-m stake, so the corresponding derived length is absent. The depth sensors on the 2-m and 3-m stakes failed to detect the ice surface, possibly because of degraded performance at low temperatures near the specified operational limits.

The BRACHI-derived lengths are broadly consistent with the tape measure, with differences up to  $\sim 3$  cm. These systematic differences are somewhat higher than those observed in lab tests and may be partially attributed to environmental sources of uncertainty, e.g., uneven ice surfaces and lower-amplitude vibrational excitations from the wind. The BRACHI measurements from  $F_1$  and  $F_2$  are self-consistent within the mean value errors, which are sub-centimeter over the two-hour observation. The errors derived from  $F_2$  are slightly smaller than those derived from  $F_1$  because of the steeper frequency-length relation of the second mode.

## 6.2 Temporal variation of measured length

Figure 6 shows BRACHI data obtained from the 2-m stake over seven days. (Limited data are available for the 1-m stake because of low wind speeds at the test site, and the batteries on the 3-m stake were inadvertently drained by repeated wireless access attempts.) Accelerometer-derived lengths computed from the first and second vibrational modes are shown separately to assess consistency and to illustrate how often each mode is excited under these particular test conditions. When both vibrational modes are present, the corresponding length calculations agree within errors. The typical uncertainties on lengths derived from  $F_1$  and  $F_2$  are 1.3 cm and 0.14 cm, respectively. In the measurement period before 2025-05-19, the internal BRACHI temperature (which is a few degrees higher than ambient) was below freezing for the majority of the time. During this period, the stake lengths display variations at the level of 1–2 cm. These variations are not statistically significant in the length data

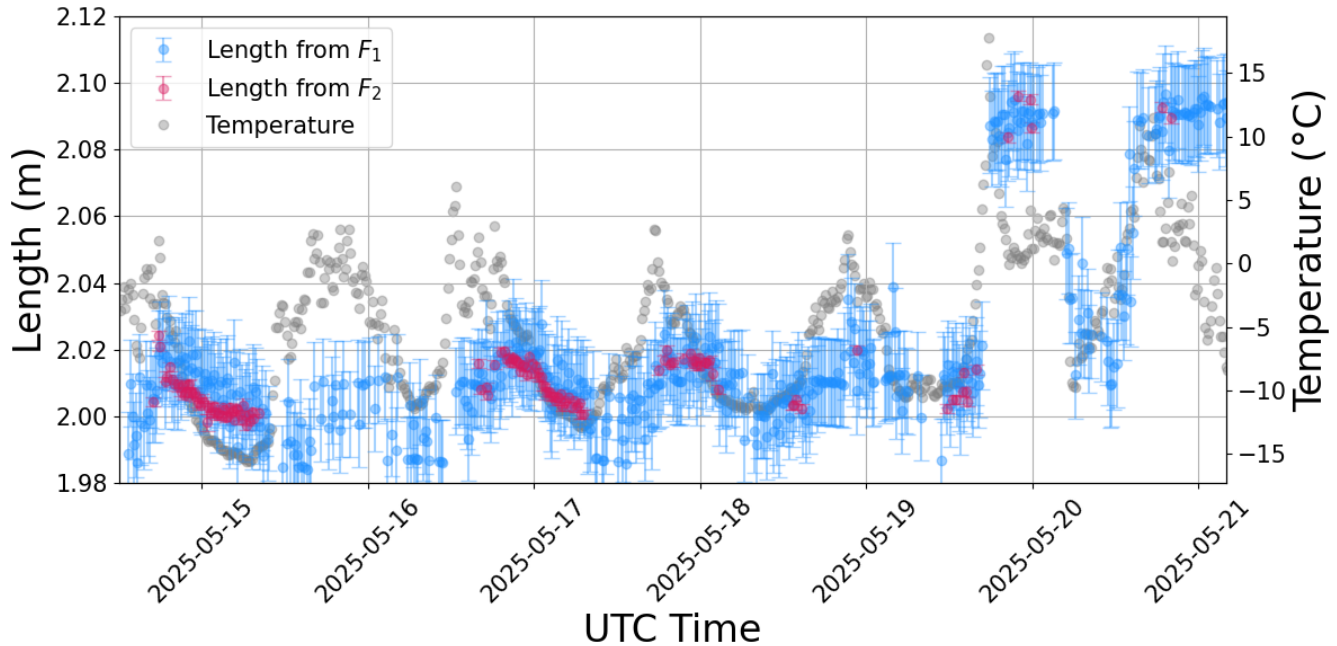


**Figure 6.** Lengths derived from accelerometer measurements for the 2-m stake over a week-long observation, with the first and second vibrational modes analyzed separately. The length measurements vary over time, tracking the changes in temperature.

derived from  $F_1$ . Although the length data from  $F_2$  have significantly smaller statistical errors, the apparent temporal variation may include temperature-dependent systematic effects at levels below the sensitivities of the accuracy tests described in §5 and §6.1. A more thorough investigation of temperature-dependent systematics will be the subject of future work. After 2025-05-19, the recorded temperature rose above freezing for longer stretches of time, and the measured stake lengths have larger temporal variations that track the temperature changes. A possible explanation is that direct sunlight warmed both the BRACHI enclosure and the stake, and heat conducted along the stakes may have created a thin layer of localized ice melt near the base. Visual inspections of the stake at the time were not performed at this level of detail, and more careful visual confirmations will be included as part of future tests.

Although the depth sensor on the 2-m stake failed to report measurements for most of the observing time, the depth sensor on the 1-m stake was largely functional and reported length measurements that qualitatively track temperature changes. The limited accelerometer data from the 1-m stake are insufficient to perform a robust comparison against the depth sensor. However, this test demonstrates that when environmental conditions allow the depth sensor to operate, the measurements serve as a valuable fallback when insufficient vibrations are excited in the stake.

## 7 Conclusions

We have conducted successful initial Arctic field tests with BRACHI and have shown that the system is capable of autonomously measuring the exposed lengths of mass-balance stakes via wind-induced vibrations. The system recorded data continuously over a week-long period during Arctic spring, and the accelerometer data yielded length measurements with centimeter-level precision, derived from the first vibrational mode. In some observing conditions when the second vibrational mode is excited, the measurement precision can improve to sub-centimeter. The length measurements from accelerometer data demonstrate the successful proof of concept of BRACHI. This system complements other automated measurement techniques of glacier surface melt by employing low-cost hardware while achieving comparable precision. Each BRACHI unit costs approximately \$50 USD, and the open-source hardware is fully serviceable.

The BRACHI depth sensor, a low-cost unit that is not rated for the full range of operating conditions, provided occasional readings that qualitatively agreed with results from the accelerometer data. We anticipate that the depth sensor will operate more reliably during the warmer Arctic summer months. This work will be the subject of a future publication that will discuss results from several BRACHI units that were installed on White Glacier during the 2025 melt season. We are currently revising the BRACHI design to incorporate an improved accelerometer and clock, reduce power consumption, increase sampling rates, and further lower the cost. Future work will include validating the new design, including more detailed tests of accelerometer systematics and temperature dependence, and additional field tests.

*Code and data availability.* The BRACHI design files, control code, analysis code, and data gathered at MARS and in the lab are available on GitHub: <https://github.com/FelixStA52/BRACHIOSAURUS> or under the following DOI: 10.5281/zenodo.18292185.

## Appendix A: Detailed calculations of vibrational frequency as a function of length

A BRACHI-equipped mass-balance stake is modeled as an extended mass at the top end of a vertical hollow cylinder, using the Euler–Bernoulli beam model. Erturk and Inman (2011) show that the exact solution for the motion of the stake yields a partial differential equation with an infinite number of vibrational eigenmodes. The corresponding eigenvalues  $\lambda_n$  solve the equation

$$1 + \cos(\lambda_n)\cosh(\lambda_n) + \lambda_n \frac{M_{\text{eff}}}{\pi L \rho (R^2 - r^2)} (\cos(\lambda_n)\sinh(\lambda_n) - \sin(\lambda_n)\cosh(\lambda_n)) = 0, \quad (\text{A1})$$

where  $M_{\text{eff}}$  is the effective mass of BRACHI,  $L$  the exposed length of the stake that is free to move,  $\rho$  the density of the stake material, and  $R$  and  $r$  are the outer and inner stake radii, respectively. The effective mass is defined as

$$M_{\text{eff}} = \int_0^L \mu(x) \phi_n^2(x) dx, \quad (\text{A2})$$

as given in Stokey (2002, ch. 29). Here,  $\mu(x)$  is the linear density of the box as a function of vertical position  $x$ , and  $\phi_n(x)$  is the mode shape of the stake for the  $n^{\text{th}}$  mode. The mode shape describes the displacement of the stake from equilibrium; the

full expression is omitted here for brevity but is available in Erturk and Inman (2011). Since  $\phi_n(x)$  and  $M_{\text{eff}}$  depend on each other, solutions for each must be obtained iteratively. Starting with  $M_{\text{eff}} = m_{\text{BRACHI}}$ , a trial mode shape is determined and used to compute a new effective mass. This process is repeated until the effective mass converges to the desired precision. The  $M_{\text{eff}}$  solution is used to solve for  $\lambda_n$  in Eq. (A1). The eigenvalues are related to the oscillation frequencies through the expression

$$\lambda_n^4 = (2\pi f_n)^2 \frac{4\rho(R^2 - r^2)L^4}{E(R^4 - r^4)}, \quad (\text{A3})$$

where  $f_n$  is the frequency of the  $n^{\text{th}}$  vibrational mode of the stake and  $E$  is the temperature-dependent Young's modulus.

*Author contributions.* FS led the development of the BRACHI hardware and software, lab tests, data analysis, and manuscript writing. HCC provided guidance on hardware implementation, analysis and interpretation of the results, and assisted with writing. JC contributed to the design and testing of the first BRACHI prototype. EE contributed to the design of the electronics and circuit board. IH provided guidance on design requirements and assisted with writing. JS provided guidance on data analysis. LT conceived the BRACHI concept, provided guidance on system requirements and glaciology applications, led the Arctic field tests, and assisted with writing.

*Competing interests.* No competing interests

*Acknowledgements.* We are extremely grateful to Brandon Ruffolo, who provided test equipment and machined the BRACHI metal cutouts late in the day right before Christmas; Ben Cheung, who helped drill the holes in several of the BRACHI enclosures; Bo Curtis, who assisted with the Arctic deployment and tests; and Maya Smith, who provided feedback on the BRACHI documentation and GitHub resources. We extend our deepest thanks to Chris Omelon for supporting our work at the McGill Arctic Research Station. We acknowledge the Polar Continental Shelf Program for providing funding and logistical support, and we extend our sincere gratitude to the Resolute staff for their generous assistance and bottomless cookie jars. We acknowledge the support of the Natural Sciences and Engineering Research Council of Canada (NSERC), RGPIN-2019-04506, RGPNS 534549-19, and USRA; New Frontiers in Research Fund, NFRFE-2021-00409; National Geographic Society Explorer Grant NGS-94983T-22. This research was undertaken, in part, thanks to funding from the Canada 150 Research Chairs Program. We thank McGill Branches for support through the IMPRESS program.

## References

Blevins, R.: Formulas for natural frequency and mode shape, New York : Van Nostrand Reinhold Co., 1979.

Bøggild, C. E., Olesen, O. B., Andreas, P. A., and Jørgensen, P.: Automatic glacier ablation measurements using pressure transducers, *Journal of Glaciology*, 50, 303–304, 2004.

Carturan, L., Cazorzi, F., Dalla Fontana, G., and Zanoner, T.: Automatic measurement of glacier ice ablation using thermistor strings, *Journal of Glaciology*, 65, 188–194, 2019.

Cogley, J., Arendt, A., Bauder, A., Braithwaite, R., Hock, R., Jansson, P., Kaser, G., Möller, M., Nicholson, L., Rasmussen, L., and Zemp, M.: Glossary of glacier mass balance and related terms, vol. 86 of *IHP-VII Technical Documents in Hydrology*, International Hydrological Programme, Paris, France, 2010.

Cremona, A., Huss, M., Landmann, J. M., Borner, J., and Farinotti, D.: European heat waves 2022: contribution to extreme glacier melt in Switzerland inferred from automated ablation readings, *The Cryosphere*, 17, 1895–1912, 2023.

Erturk, A. and Inman, D. J.: Appendix C: Modal Analysis of a Uniform Cantilever with a Tip Mass, in: *Piezoelectric Energy Harvesting*, John Wiley & Sons, Ltd, ISBN 9781119991151, [https://doi.org/https://doi.org/10.1002/9781119991151.app3](https://doi.org/10.1002/9781119991151.app3), 2011.

Hugonet, R., McNabb, R., Berthier, E., Menounos, B., Nuth, C., Girod, L., Farinotti, D., Huss, M., Dussaillant, I., Brun, F., and Kääb, A.: Accelerated global glacier mass loss in the early twenty-first century, *Nature*, 592, 726–731, <https://doi.org/10.1038/s41586-021-03436-z>, 2021.

Hulth, J.: Using a draw-wire sensor to continuously monitor glacier melt, *Journal of Glaciology*, 56, 922–924, 2010.

Immerzeel, W., Lutz, A., Andrade, M., Bahl, A., Biemans, H., Bolch, T., Hyde, S., Brumby, S., Davies, B., Elmore, A., Emmer, A., Feng, M., Fernández, A., Haritashya, U., Kargel, J., Koppes, M., Kraaijenbrink, P., Kulkarni, A., Mayewski, P., and Baillie, J.: Importance and vulnerability of the world's water towers, *Nature*, 577, <https://doi.org/10.1038/s41586-019-1822-y>, 2020.

Landmann, J. M., Künsch, H. R., Huss, M., Ogier, C., Kalisch, M., and Farinotti, D.: Assimilating near real-time mass balance observations into a model ensemble using a particle filter, *The Cryosphere Discussions*, 2020, 1–34, 2020.

Pollard, W., Haltigin, T., Whyte, L., Niederberger, T., Andersen, D., Omelon, C., Nadeau, J., Ecclestone, M., and Lebeuf, M.: Overview of analogue science activities at the McGill Arctic research station, axel heiberg island, canadian high arctic, *Planetary and Space Science*, 57, 646–659, 2009.

Sharp, M., Burgess, D. O., Cogley, J. G., Ecclestone, M., Labine, C., and Wolken, G. J.: Extreme melt on Canada's Arctic ice caps in the 21st century, *Geophysical Research Letters*, 38, <https://doi.org/https://doi.org/10.1029/2011GL047381>, 2011.

Stewart, R. D., Hut, R., Rupp, D. E., Gupta, H., and Selker, J. S.: A resonating rainfall and evaporation recorder, *Water Resources Research*, 48, <https://doi.org/https://doi.org/10.1029/2011WR011529>, 2012.

Stokey, R.: Vibration of Systems Having Distributed Mass and Elasticity, in: *Harris' Shock and Vibration Handbook*, 5th Edition, edited by Piersol, A. G. and Paez, T. L., McGraw-Hill, 2002.

Summers, P. T., Chen, Y., Rippe, C. M., Allen, B., Mouritz, A. P., Case, S. W., and Lattimer, B. Y.: Overview of aluminum alloy mechanical properties during and after fires, *Fire Science Reviews*, 4, 3, 2015.

Timoshenko, S.: On the transverse vibrations of bars of uniform cross-section, *The London, Edinburgh, and Dublin Philosophical Magazine and Journal of Science*, 43, 125–131, <https://doi.org/10.1080/14786442208633855>, 1922.

Wickert, A. D., Barnhart, K. R., Armstrong, W. H., Romero, M., Schulz, B., Ng, G.-H. C., Sandell, C. T., La Frenierre, J., Penprase, S. B., de Vries, M. V. W., et al.: Automated ablation stakes to constrain temperature-index melt models, *Annals of Glaciology*, 64, 425–438, 2023.

Østrem, G. and Stanley, A.: Glacier mass-balance measurements: a manual for field and office work, Department of Mines and Technical Surveys, Glaciology Section, 1966.